Structural electrical anisotropy in the crust at the South-Central Chilean continental margin as inferred from geomagnetic transfer functions

Heinrich Brasse, Gerhard Kapinos, Yuguo Li, Lutz Miitschard, Wolfgang Soyer, Diane Eydam

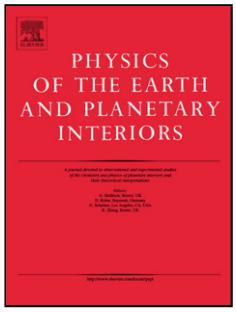

Title: Structural electrical anisotropy in the crust at the South-Central Chilean continental margin as inferred from geomagnetic transfer functions

Authors: Heinrich Brasse, Gerhard Kapinos, Yuguo Li, Lutz Miitschard, Wolfgang Soyer, Diane Eydam

PII: S0031-9201(08)00314-2
DOI: doi:10.1016/j.pepi.2008.10.017
Reference: PEPI 5094

To appear in: *Physics of the Earth and Planetary Interiors*

Received date: 23-2-2008
Revised date: 27-9-2008
Accepted date: 15-10-2008

Please cite this article as: Brasse, H., Kapinos, G., Li, Y., Miitschard, L., Soyer, W., Eydam, D., Structural electrical anisotropy in the crust at the South-Central Chilean continental margin as inferred from geomagnetic transfer functions, *Physics of the Earth and Planetary Interiors* (2008), doi:10.1016/j.pepi.2008.10.017

Structural electrical anisotropy in the crust at the South-Central Chilean continental margin as inferred from geomagnetic transfer functions

Heinrich Brasse *, Gerhard Kapinos, Yuguo Li [1], Lutz Mütschard, Wolfgang Soyer [2], Diane Eydam

Freie Universität Berlin, Fachrichtung Geophysik, Malteserstr. 74-100, 12249 Berlin, Germany

Abstract

Induction vectors, as a visualization of geomagnetic deep sounding transfer functions, display an unique pattern at the South Chilean continental margin between latitudes 38-41°S and longitudes 71-74°W: At long periods of approx. 3 000 s their real parts are uniformly deflected from the W-E direction (which would be expected due to the coast effect and/or anomalies beneath the roughly N-S striking Andean mountain chain) to the NE. Attempts to model this behavior with simple and geologically realistic 3-D models failed, but a reasonable data fit was obtained by employing 2-D models with a structurally anisotropic, lower crust. This anisotropy hints at a deeply fractured, fluid-rich crust with a major strike direction of 40-50° (SW-NE), oblique to the continental margin and in accordance with the regional stress field in the region of the volcanic arc. A surprising result is that the anisotropy persists in the forearc and may even reach until the continental slope near the trench.

Key words: Geomagnetic induction, Subduction zone processes, Anisotropy, South America

* Corresponding author
Email addresses: h.brasse@geophysik.fu-berlin.de (Heinrich Brasse), kapinosg@geophysik.fu-berlin.de (Gerhard Kapinos), yuguo@ucsd.edu (Yuguo Li), muetschard@geophysik.fu-berlin.de (Lutz Mütschard), wsoyer@milan.westerngeco.slb.com (Wolfgang Soyer), diane@geophysik.fu-berlin.de (Diane Eydam).
[1] now at Scripps Institution of Oceanography, La Jolla
[2] now at WesternGeco-Geosystem, Milano

1 Introduction

Magnetotelluric (MT) transfer functions are commonly displayed as apparent resistivities and phases, both derived from the ratio of horizontal electric and magnetic fields (impedance). If the vertical magnetic field has been measured as well, the transfer function between vertical and horizontal magnetic fields (often termed "tipper" because the secondary field of a lateral conductivity variation tilts the magnetic field out of its horizontal direction in a one-dimensional setting) may additionally be used to derive an image of electrical conductivity in the earth:

$$B_z(T) = W_x(T)B_x(T) + W_y(T)B_y(T), \tag{1}$$

where x,y,z denote cartesian, geomagnetic coordinates, B is geomagnetic induction and T is period. To distinguish it from MT sensu strictu this method is often referred to as Geomagnetic Deep Sounding (GDS).

The complex-valued tipper $\mathbf{W} = (W_x, W_y)^t$ (t denotes transpose) is conveniently displayed as an "induction vector" or "arrow" for both real and imaginary parts, calculated according to:

$$\vec{P}(T) = Re\{W_x(T)\}\vec{e}_x + Re\{W_y(T)\}\vec{e}_y \tag{2}$$

$$\vec{Q}(T) = Im\{W_x(T)\}\vec{e}_x + Im\{W_y(T)\}\vec{e}_y, \tag{3}$$

with $\vec{e}_x$ and $\vec{e}_y$ as unity vectors in x- and y-direction. Plotted on a map and if only a single, two-dimensional conductivity anomaly is present, real vectors point away from regions of enhanced conductivity, while imaginary vectors change sign at a period where the real parts are maximal. We employ the

commonly used term "vector" here, but note that this expression should be used with care when several induction anomalies are coupled (Siemon, 1997).

For reasons of simplicity presentation of real parts is usually preferred; plotting real vectors in unrotated coordinates is often referred to as "Wiese convention" (Wiese, 1962). At an ocean margin induction vectors (should) point away from and perpendicularly to the coastline due to the high conductivity of seawater in the range of $\sigma = 3\,\mathrm{S/m}$; this is the so-called "coast effect", which may be observable far inland dependent on the resistivity (reciprocal of σ) of the continent.

This simple image is obscured if conductivity distribution is 3-D and/or anisotropic. Then conclusions concerning electrical strike directions may not be drawn intuitively any more; this became particularly evident at the Chilean continental margin, where – despite of the elongated, 2-D appearance of the coastline over thousands of kilometers – induction vectors in many near-coastal regions do not point away from the coast, but rather obliquely or even parallel to it.

2 Geological background and experiment layout

We report here on observations in South-Central Chile between latitudes 38°S and 41°S (Fig. 1), where the oceanic Nazca plate is subducted beneath the South American continent and the great earthquake of 22 May 1960 (moment magnitude $M_w = 9.5$) initiated (Cifuentes, 1989). Subduction is oblique with an angle of ∼25° (i.e., N77°E) with respect to the plate margin and with a current velocity of ∼6.5 cm/a (Klotz et al., 2006). The study area is located in the northernmost Patagonian (Neuquén) Andes and can be subdivided into

several main morphotectonic units (e.g., Folguera et al. (2006); Melnick et al. (2006)): 1) a narrow Coastal Platform comprising uplifted Tertiary marine and coastal sequences; 2) the Coastal Cordillera, formed by a Permo-Triassic accretionary complex and a late Palaeozoic magmatic arc; 3) the Longitudinal Valley, a basin filled with Oligocene-Miocene sedimentary and volcanic rocks, covered by Pliocene-Quaternary sediments; 4) the Main Cordillera, formed by the modern magmatic arc and intra-arc volcano-sedimentary basins; 5) the Loncopué Trough, already in Argentina, an extensional basin east of the Main Cordillera associated with abundant mafic volcanism; 6) the southern extension of the Agrio fold-and-thrust belt; and 7) the Mesozoic Neuquén Basin and the Cretaceous-Tertiary foreland basin to the east.

Subduction at the Chilean margin started already in the late Paleozoic, while Andean evolution began in the Jurassic, associated with the opening of the South Atlantic Ocean. In the Cretaceous widespread plutonism occurred in the Coastal Cordillera and in the area of the volcanic arc, where the Patagonian Batholith was formed. South of 38°S the position of the volcanic arc remained relatively constant through time with the exception of a significant broadening of the magmatic system (Muñoz et al., 2000) and an 80-100 km westward shift of the volcanic front in the late Oligocene-early Miocene with respect to its current position (Parada et al., 2007). This event was probably related to the breakup of the Farallon plate into Nazca and Cocos plates, respectively, and subsequent changes in plate convergence and subduction angle (Muñoz et al., 2000). For further description of the tectonic evolution see the overview articles by Stern (2004), Ramos and Kay (2006) and Glodny et al. (2006).

The modern Principal Cordillera is dominated by the Holocene volcanoes of the Southern Andean Volcanic Zone, with some of the most active volca-

noes in South America, e.g., Villarrica, Llaima and Lonquimay (Gonzáles-Ferrán, 1994). The chain of stratovolcanoes is aligned parallel to the trench and along the Liquiñe-Ofqui Fault (LOF), a mega shear zone extending for over 1 000 km from the triple junction of Antarctic, South American and Nazca plates to ∼38°S (Cembrano et al., 1996, 2007). A NW-SE – thus obliquely to the trench – oriented fault system crosses the arc and forearc (e.g., Melnick et al., 2006), which may have been of importance for a major eruption in the Cordon Caulle volcanic complex immediately after the $M_w = 9.5$ earthquake (Lara et al., 2004). The Lanalhue Fault, in particular, is regarded as an inherited, continuously reactivated, pre-Andean structure, which is associated with deep-reaching seismicity (Yuan et al., 2006).

Two long-period magnetotelluric campaigns were conducted, an earlier one in 2000 and an additional field experiment in austral summer 2004/2005, which also included an amphibious component employing sea-bottom instruments from Woods Hole Oceanographic Institution (WHOI). While the first experiment (Brasse and Soyer, 2001; Soyer, 2002) was carried out in the framework of the multi-disciplinary programme SFB 267 "Deformation Processes in the Andes", the second one (Kapinos and Brasse, 2006) was part of the TIPTEQ project ("From the Incoming Plate to Megathrust Earthquakes"), with other subprojects dealing with passive and active seismology, gravity and geology/tectonics. Structural information at the South Chilean margin in the study area concerning Moho depths and geometry of the downgoing plate may particularly be inferred from a large number of recent seismic experiments (Bohm et al., 2002; Lüth and Wigger, 2003; Rietbrock et al., 2005; Haberland et al., 2006; Krawczyk et al., 2006).

During the two campaigns, a total of 72 stations were deployed between the

Argentinian border and the Pacific Ocean, yielding electromagnetic (MT and GDS) transfer functions in the period range between 10 s – 20 000 s. On land, the network encompasses the areas of the Coastal Cordillera, the Central Depression or Longitudinal Valley and the Principal Cordillera (see Fig. 1). The seafloor stations (from Woods Hole Oceanographic Institution) were deployed across the Peru-Chile trench during R/V Sonne cruise SO181. Since analysis of offshore sites is not completed yet, we restrict the following study to the onshore component of the experiment.

3 2-D modeling – the standard isotropic approach

An early modeling approach by inverting only impedance data was carried out by Brasse and Soyer (2001) for the central profile at 38.9°S in Fig. 1, which corresponds to the seismic ISSA line (Lüth and Wigger, 2003). The major result was the detection of a good conductor beneath the Central Valley, probably associated with the Lanalhue Fault (formerly known as Gastre FZ, obliquely traversing the northern Patagonian Andes in a SE-NW direction), and a high conductivity zone beneath the volcanic arc.

We extended this modeling study by incorporating tipper transfer functions and known a-priori information like highly accurate swath bathymetry data, obtained during several cruises of R/V Sonne (Scherwath et al., 2006); the result is shown in Fig. 2. Another feature included in the starting model is a highly-resistive slab of the subducted Nazca Plate, an assumption justified by EM measurements on the seafloor (Chave et al., 1991). As in the previous model a common strike direction of 0° was assumed, justified by multi-site, multi-frequency analysis of strike directions according to Smith (1997). Regu-

larized inversion was carried out with the non-linear conjugate gradient code of Rodi and Mackie (2001); the regularization parameter was set to $\tau = 10$. Error floors were set to 20% for apparent resistivities, 5% for phases, and 0.1 (absolute value) for real and imaginary parts of the tipper. Since tipper data are not consistent with impedance strike directions (see below), we used their projection on the y-(EW-)axis. Further details concerning inversion settings and sensitivity issues, which reach beyond the purpose of the study presented here, are described by Kapinos (2008).

In terms of a root mean square error, the obtained data fit is remarkably good with a rms = 1.1; but note that this is mainly due to the relatively high error floor assigned to the tipper data. However, model structures do not change significantly if a different weighting of data relative to each other is applied (Kapinos, 2008). Furthermore, the main structures are only marginally affected, if different starting models are used (e.g., a homogeneous half space with the Pacific Ocean included). Since isotropic modeling is not the main topic of the study presented here, we skip discussion of data fit and sensitivities here and just investigate the major features of the model.

As in Brasse and Soyer (2001) the main conductors (B, C and C' in Fig. 2) are located beneath the Central Valley and the volcanic front. The highly-conductive zone C at mid-crustal depths beneath the volcanic arc seems particularly interesting: The profile runs just south of Llaima volcano, and the model may simply image a large magma deposit beneath, but offset by $\sim$10 km to the east. Note that Llaima erupted violently on 1 January 2008 at the time of preparation of this manuscript, but also note that these data were collected already in 2000, and it is of course not known how this eruption may have affected the conductor by removing or relocating a significant part of the magma

deposit.

The Central Valley conductor on the other hand, beneath the trace of the Lanalhue Fault, is unlikely to originate from partial melts due to temperature considerations in the (relatively cold) forearc – fluids are seen here as the main cause of elevated conductivities. A consistent feature is conductor D east of the eastern margin of the profile (already in Argentina) – although not truly resolved with respect to location and resistivity due to the lack of stations, it appears in all inversion runs. A preliminary explanation may lie again in a root zone for the Holocene backarc volcanism in the Loncopué Trough. However, only a future extension of the profile into Argentina could unambiguously answer this question.

A very good conductor (A) appears west of the profile already beneath the ocean, overlying the downgoing plate. This structure is not seen when only crude bathymetry is taken into account (Brasse and Soyer, 2001) – this underlines the importance of exact bathymetry for near-coastal data. It may at first glance seem like an inversion artifact; however, it is also modeled at the northernmost TIPTEQ profile, where an additional offshore station was incorporated (Kapinos, 2008). Furthermore, it correlates with a strong seismic reflector (Groß et al., 2007) beneath the TIPTEQ traverse. The origin of this structure remains enigmatic for the time being, but analysis of seismic tomography data suggests a possible low-velocity zone (Haberland, pers. comm.) and thus a fluid-rich accretionary wedge, perhaps fed by faults originating at the downgoing plate. Interestingly, the overall appearance of the model with its several conductors – particularly structure A off the coast – is quite similar to a model recently published by Soyer and Unsworth (2006) for the Cascadia subduction zone in SW Canada.

The subducted Nazca plate was modified in the course of the inversion process, leading to a much more heterogeneous image of the slab; additionally several poor conductors are now seen in the continental crust, rising from the plate interface. Apart from the main features in Fig. 2, minor structures also include the near-surface, but not-deep reaching sediments in the Central Valley in accordance with tectonic assumptions (H. Echtler, pers. comm.).

Although the 2-D inversion model appears like a plausible result particularly with respect to the resolved conductive features beneath the profile, it cannot represent a "true" model in an important aspect: its response only approximates the vertical magnetic field data, which are significantly and systematically distorted throughout the study area. Furthermore, the number of conductive "blobs" of the model, resembling the study of Heise and Pous (2001), suggest a different, anisotropic approach. This is treated in the following sections.

4 GDS transfer functions in South-Central Chile

The Chile trench reaches a depth of ∼4 600 m in the study area, yielding a conductance of 14 000 S (Siemens); taking into account the – presumably well-conducting – sedimentary filling this value should even be higher. Tipper magnitude directly at the coast is $W \approx 0.8$ for long periods. This is not as large as would be the case near a deep ocean if the continental lithosphere would in total be highly-resistive (i.e., resistivity in the order of 1 000 Ωm or more). Thus the continent must generally be less resistive (a few hundred Ωm maximum) or must at least contain anomalous high-conductivity zones.

Given the average N10°E trend of the trench and the similar overall course of the volcanic chain, it was expected that real parts of induction vectors would show a general W-E tendency. This is, however, not the case. Instead, at long periods, all real induction vectors point systematically NE for all sites in the measuring area, regardless on which geological unit data were collected (Fig. 3). Note that there is not a single site in the study area where this observation is opposed. Thus flow of anomalous current in the continent – itself caused by current concentration in the ocean parallel to the coast – is not NS as would be the case for a simple 2-D distribution of conductivity, but obliquely deflected on a large lateral scale.

On the other hand, this effect is not observed at shorter periods: The coast effect is "normal" and vectors in the Coastal Cordillera point roughly perpendicularly away from the shoreline (not necessarily perpendicular to the trench, since local bathymetry is dominating at short periods). This also rules out an instrumental effect as we initially suspected (and which gave rise to a later extensive test program of stations near Niemegk geomagnetic observatory close to Berlin). Source effects should not play a significant role, too, because the study area is located in mid-latitudes and far from both polar and equatorial electrojets.

An interesting effect is visible around highly active volcanoes Villarrica (altitude 2 847 m) and Llaima (3 125 m, latest eruption in 2008), where a small network of sites was established: While induction vectors at 100-200 s point away from Villarrica at the closest sites, this is not seen at Llaima. Although all volcanic edifices lead to a topographic effect at their slopes, this cannot be the reason for the direction and magnitude of vectors at Villarrica. Since the slope of this mountain is only in the order of 25-30°, topography signals in

MT transfer functions are restricted to short periods (<10 s) and only a static shift-like effect remains in apparent resistivities as was shown by 2-D and 3-D modeling of topographic effects in the central Andes (Eydam, 2008; Brasse and Eydam, 2008). We may thus assume that deeper in the crust beneath Villarrica a large-scale magma deposit might exist – note that the crater at the top of Villarrica is filled with a lava lake (Calder et al., 2004). A more detailed statement about conductivity distribution at depth below the volcano is not possible for the time being, since detailed 3-D modeling has not been carried out yet. Note that these long-period data only permit statements about the deeper crust; to assess a possible magma deposit just beneath the volcanic edifices would require measurements at shorter periods (AMT range) on a denser network.

5 3-D modeling attempts to explain induction vectors

It is obvious that the anomalous deflection of induction vectors cannot be explained by pure 2-D models. We therefore tested several simple 3-D approaches to account for the deflection over a large area, in particular the N-S extent of at least 350 km (it is not known if transfer functions continue to be this anomalous to the north and south of the measuring area, but this may quite safely be assumed at least for some distance). Such models must incorporate the Pacific Ocean with an average depth of ∼4.5 km and an almost N-S running coastline, and some other structure of large, regional extent which accounts for the deflection. For the computations the algorithm of Mackie et al. (1994) was applied; seawater resistivity was fixed at $\rho = 0.3\,\Omega$m.

Test 1: It may be possible that a layer with increasing conductance (conductivity-

thickness product) from south to north exists at some depth in the crust or even in the upper mantle. This may indeed explain the induction vectors but leads to inherently large conductances in the northern part (and unrealistic conductivities if layer thickness is not changed accordingly). Furthermore there exists no geological evidence whatsoever for such a layer and the idea is thus abandoned here.

Test 2: South of the southernmost site begins archipelagic Chile, i.e., the Central Depression is submerged and the Coastal Cordillera becomes a chain of islands, with Isla de Chiloé being the largest (not shown in Fig. 1). The distribution of seawater masses causes therefore a deflection of induction vectors near latitude 41°S, but according to our model results this effect does not reach far enough to the north, taking the known water depths into account.

Test 3: At 45-46°S, i.e., 450-550 km south of the study area the Chile Rise is subducted beneath the continent; this is the triple junction between Antarctic, Nazca and South American plates. It may be speculated that the location of the triple junction is associated with a deep seated plume structure of enhanced conductivity. Such a hypothetic good conductor (resistivity 1 Ωm) was incorporated into the 3-D model (which also takes the irregular coastline into account); the response is shown in Fig. 4. Again, the model response is only compatible with the data at the southernmost sites of the measuring area; in the north vectors point strictly W-E.

Summarizing, simple and (geologically) realistic 3-D models explaining the observed induction vectors could not be found (which does of course not exclude more detailed classes of models, see later). We therefore tested another approach, the simulation of a deeply fractured crust with anisotropic 2-D

models.

6 2-D models with anisotropy: some principal considerations

Under anisotropy we may either understand micro-anisotropy as an inherent rock property or structural (pseudo- or macro-) anisotropy; in both cases the inductive scale length ("wave length") of fields in the earth is larger than the width of individual structural units which are thus not resolvable separately. We may assign either one or two directions to high conductivity: The first case may be interpreted as simulating a system of line currents while the second may be regarded as an image of a sequence of fault planes. A ratio of $\gg$100 between directions of low and high conductivity seems reasonable if we assign the resistive part to the host rock and the conductive one to possible fault planes, assumed to be fluid-rich in the damage zone of the fault core.

Full anisotropy has to account for 6 variables, the 3 principal resistivities, strike, dip and slant (cf., Pek and Verner, 1997). Due to the resulting complexity we varied only the first 4 parameters leaving dip and slant constant at 90° and 0°, respectively. Dip and slant (if not too large) have a much smaller influence on transfer functions than the other parameters. Since ρ_z has only minor influence on induction vectors at least distant from the coast, this quantity was set equal to ρ_x for most model experiments.

If an anisotropic layer – extending to infinity in horizontal directions – is present in an otherwise isotropic and homogeneous or layered half space, a split of impedance phases and apparent resistivities is observed while the vertical magnetic field is zero; the vertical components of the secondary field from the

parallel current lines – or planes – superpose destructively. A vertical field only arises if the anisotropic layer is bounded or if some other lateral inhomogeneity is present, in our case mainly from the coast effect at the Chilean margin. Under 2-D isotropic conditions only the W_y component of the tipper would exist due to the basically N-S trending coastline and trench. Here, however, W_x is of similar magnitude at long periods.

First we evaluate the responses of several principal models as outlined in Fig. 5. The following plots (Fig. 6) are for periods of T = 102.4 s and 3277 s, respectively, corresponding to period bands at which transfer functions are estimated by the time series analysis scheme. We thus analyze responses at periods corresponding to relatively short and large penetration depths. Calculations were carried out employing the algorithms of Pek and Verner (1997) and Li (2002); both yield comparable results.

(1) An anisotropic layer between z = 5 km and 20 km, bounded at y = 20 km and y = 200 km is embedded in a homogeneous half space of resistivity 300 Ωm. Resistivities of the layer are set to $\rho_x = \rho_z = 1\,\Omega$m and $\rho_y = 300\,\Omega$m, anisotropy strike to $\alpha = 45°$. The conductive axis thus strikes SW-NE. We neglect any non-zero dip or slant and simply assume vertical conductive planes. Vertical resistivity has only minor influence on the vertical magnetic field at the surface (in contrast to impedance, which we don't further investigate here) and only near the layer boundaries. The response of this model is shown in Fig. 6: At both margins of the anisotropic block significant induction vectors are observed, pointing NW in the west and SE in the east (i.e., both perpendicular to strike); above the center of the block the combined effect of both margins results in a vanishing vertical field. According to depth of penetration vectors are largest for shorter periods – for longer periods penetration depth increases

and the layer is too shallow to have a major effect.

(2) Since the observed induction vectors display a significant W_x component from the coast until the Argentinian border, the anisotropy has to persist eastward beyond the station network. This is taken into account by removing the layer bound in the east. Because no data exist in Argentina at this latitude, we have no information on the eastern margin of the layer and simply set it to infinity. Furthermore, a large W_x component is present also at coastal site PUR and even at sea-bottom site OB7 20 km offshore on the northern profile (Kapinos and Brasse, 2006) as well as on Isla Mocha (O. Ritter, pers. comm.). Therefore the western margin has to be extended below the ocean; here it is arbitrarily set to y = -20 km. As expected, oblique induction vectors are only observed at the western margin, but now the effect is largest for long periods due to the infinite extent towards east.

(3) The Pacific Ocean is simulated by a conductive half layer with a thickness of 5 km. For the time being we neglect the actual bathymetry and place the block at y = -80 km from the coast, i.e., 60 km away from the anisotropic layer. We also neglect dependence of seawater conductivity on salinity and temperature (i.e., water depth) and set it to an average value of $\sigma = 3.3\,\mathrm{S/m}$ ($\rho = 0.3\,\Omega\mathrm{m}$).

The third model already grossly explains the observed induction vectors at long periods: They point NE over the whole profile, slowly decreasing in length with distance from the ocean. This behavior is not difficult to understand: If ocean and anisotropic layer are separated far enough from each other and thus not coupled, we may simply carry out a vector addition of contributions originating from the ocean and the layer, respectively (Fig. 7). Accordingly

the E-pointing "ocean vector" and the NW-directed "anisotropy vector" yield a combined vector pointing towards NE. Both real parts of W_x and W_y are positive in this case. At short periods the ocean effect is smaller due to the distance from the ocean with its crude geometry adopted here (note that this characteristic does not conform with observation and a more realistic bathymetry has to be incorporated; see below). Imaginary parts remain small in all cases, they are discussed later.

If, however, the anisotropic layer extends below the ocean, the anomalous fields of both structures will be coupled. Then a simple vector addition does not suffice; e.g., the secondary field of the anisotropic layer induces a "secondary secondary" field in the ocean which is no longer N-S but rather obliquely oriented with respect to the coast. This is taken into account by the modeling algorithm (Fig. 7). For further discussion on coupled anomalies in the anisotropic case see, e.g., Weidelt (1999) and Soyer (2002).

From these fundamental considerations it is immediately evident, that the anisotropy strike does *not* reflect the NW-SE oriented fault pattern as displayed in Fig. 1. Highly conductive planes in that direction would produce SE-oriented induction vectors; thus information from tippers reveals other, less obvious structures (see discussion below).

(4) As already mentioned above, the uniform pattern of induction vector deflection is only observed at periods $> 1\,000$ s, while at shorter periods local effects come into play. In a 4th test we thus shifted the anisotropic layer into the lower crust, i.e., it is located now between 20 and 38 km. As can be seen in Fig. 6, this approach also reproduces the oblique vectors and differences to the responses of model (3) are only minor. It is thus difficult to discriminate

between upper and lower crustal anisotropy from one period alone, and the full period range has to be taken into account.

7 Anisotropic models for the Chilean margin

Due to the large number of parameters involved when carrying out 2-D anisotropic modeling, the search for a model that fits real and imaginary tippers at all sites for all frequencies, and that is preferably somehow geologically realistic is a time-consuming issue. Like in the preceding section we set slant, dip to constant values and varied only ρ_x, ρ_y (with $\rho_z = \rho_x$) and anisotropy strike α plus the isotropic background resistivities. Some of the features of the isotropic 2-D inversion results (see Fig. 2) were incorporated and adjusted where necessary.

The resulting model is displayed in Fig. 8 – calculated for the central profile of Fig. 1. It incorporates a homogeneous background with a resistivity of 200 Ωm, an anisotropic layer in the lower crust and the Pacific Ocean with detailed bathymetry, taken from ETOPO2 data and swath bathymetry obtained during several cruises of R/V Sonne (Scherwath et al., 2006). The subducting oceanic Nazca slab is modeled as a poor conductor with a vertical extent of 150 km (lower limit not shown in Fig. 8). The dip angle of the slab is provided by seismological studies (Bohm et al., 2002; Yuan et al., 2006) and the TIPTEQ seismic transect along the northern MT profile (Groß et al., 2007).

The trench contains a sediment filling with a thickness of about 2 km (Völker et al., 2006) and with presumably low (but unknown) resistivity. The filling and its geometry – known from offshore reflection seismology (e.g., Sick et al., 2006) – is roughly taken into account by assigning an arbitrary low resistivity

(5 Ωm), which suffices if only onshore (i.e., far away) stations are investigated. The same resistivity is set for the uppermost oceanic crust. We used also information from the isotropic inversion; particularly the near surface structures are motivated by isotropic models and allowed to fit at least in a crude manner the short-period induction vectors. On the other hand the compatibility between the isotropic and anisotropic models shows that they complement rather than oppose each other.

We carried out numerous tests to constrain upper and lower boundaries of the anomalous, anisotropic layer. Without going into further detail here it may be concluded that one cannot resolve (as might be expected) the thickness of the anisotropic layer; in our model it reaches until Moho depths. The crust-mantle boundary lies at 35-45 km depth in South Chile as inferred from seismological studies (e.g., Krawczyk et al., 2006; Asch et al., 2006). Since the deflection of induction vectors persists for offshore stations until the trench (Kapinos and Brasse, 2006), the anisotropic layer may not be located at mantle depths, because the downgoing slab would cut this layer apart. It is additionally not easy to constrain the upper limit of the layer since, at short periods, induction vectors show more local (also 3-D) features which are difficult to implement.

It would be unrealistic to assume that in a subduction zone setting (considering the movement of plates, resulting stress field and the oblique faults traversing the study area) the anisotropic layer will stay intact (unharmed) at the regional scale. It is rather to expect that features like resistivity or strike direction will change along the profile and which will also be reflected in the induction vectors. Indeed, the best fitting is obtained by dividing the anomalous layers in sections with minor variations in the anisotropic parameters. The values of resistivities in x-, y- and z-directions and the strikes are shown

in Fig. 8. The ocean primarily accounts for the length of induction vectors near the coast while the strike of anisotropy is responsible for the deflection from W-E. The minimum of vector lengths at ∼75 km may be accounted for by introducing a homogeneous and isotropic block at the location where the profile crosses the Lanalhue Fault, in accordance with the isotropic inversion results.

In the model of Fig. 8 this anisotropy strike – i.e., the conductive axis – is basically running NE-SW. This strike direction is also motivated by the horizontal stress field and lineaments of minor eruptive centers along the Liquiñe-Ofqui lineament (López-Escobar et al., 1995), which is discussed later.

Note that MT and GDS data are usually measured in geomagnetic coordinates and the coordinate system used here is set accordingly. Since the declination of the main geomagnetic field is in the order of N10°E (incidentally similar to the direction of the trench and the volcanic chain), it has to be taken into account when comparing geomagnetic results with geographic directions. A geomagnetic strike direction of 50° thus corresponds to geographic N60°E.

Also note that anisotropy persists along the whole profile and extends below the volcanic arc (where induction vectors are small but still deflected) and even into Argentina, east of the easternmost site location. Introducing an isotropic good conductor below or to the east of the profile levels the amount of induction vectors and debases the fitting considerably. The model in Fig. 8 also includes near-surface, well-conducting sediments ($\rho = 40\,\Omega$m with a very thin layer of resistivities of $10\,\Omega$m on top, which is not visible in the plot) in the Central Depression and the Bío-Bío valley. The thickness of these sediments is not known and was arbitrarily set to 2 km. Finally, Fig. 9 shows the modeled

and measured transfer functions for real and imaginary parts at all periods along the central profile. Apart from responses at short periods (and at long periods for the imaginary part) the data fit is reasonable.

We can of course not rule out that a certain degree of anisotropy exists in the uppermost continental mantle or in parts of the upper crust. In the 1st case this is not resolvable, in the 2nd case a possible difference between ρ_x and ρ_y could be so small that it has only negligible influence. We may also discard a possible anisotropy of the oceanic crust (which might intuitively be the case due to the numerous fracture zones entering the subduction system) as the cause for induction vector deflection – model studies showed that its influence would not reach far enough along the profile on the continent.

8 Discussion

The deduced overall preference direction of electrical conductivity (NE-SW) does not agree with the image of faults in the South-Central Andes, striking obliquely (NW-SE) to the continental margin as shown in Fig. 1 (Melnick et al., 2006), as could originally be suspected. Apart from the Lanalhue Fault – consistently modeled as a good conductor in both isotropic and anisotropic approaches – the strike direction in the lower crust is rather perpendicular to the overall forearc fault pattern. The (structural) deep-crustal anisotropy also crosses the most prominent mega shear zone in Chilean Northern Patagonia, the ∼N10°E striking Liquiñe-Ofqui Fault Zone (LOF) which extends from the triple junction area at ∼46°S until 38°S, where it terminates at the Bío-Bío-Aluminé Fault (BBAF). The LOF is assumed to largely control volcanism in S. Chile (e.g., Cembrano et al., 1996) because many of the Quaternary and

active volcanoes are aligned along this lineament.

The structural anisotropy has to continue eastwards across the border into Argentina for at least several tens of kilometers, perhaps until the backarc volcanic centers of the Loncopué trough. The lateral extent to the east cannot be constrained, as there are no stations at this latitude in Argentina (the closest stations from the University of Washington and INGEIS Buenos Aires are still several hundred km to the north; J.R. Booker and C. Pomposiello, pers. comm.). On the other side of the Andean range, the anisotropy reaches most likely until the plate interface, at least significantly beneath the Pacific Ocean. The N-S extension of the anomalous zone is again not known due to missing data N of 38°S and S of 41°S.

A hint at the cause of the structural anisotropy comes from an early observation by Nakamura (1977): Different from the ∼N10°E alignment of the large stratovolcanoes along the LOF, minor eruptive centers, parasitic vents and flank craters in the Central Southern Volcanic Zone are predominantly aligned in a NE-SW direction. Nakamura (1977) related this preference direction to the maximum horizontal stress S_H in the arc region and assumed a system of dikes enabling the rise of molten or partially molten material to the surface. López-Escobar et al. (1995) and Muñoz et al. (2000) refined this study by analyzing the geochemistry of rocks and their source region. Indeed, most of the samples they analyzed are of mainly basaltic composition (in contrast to the more andesitic-basaltic composition of the large stratovolcanoes), indicating a short residence time of magmas in the crust. The generally NE-SW oriented stress in this part of the Chilean margin (Assumpcão, 1992) was recently confirmed by Reuther and Moser (2007) for the uppermost crust until depth of ∼500 m. The analysis of 2nd order structures (lineaments, dikes,

drainage anomalies) by Rosenau et al. (2006) gives further evidence of the importance of the NE-SW direction.

According to Shaw (1980) dikes in the crust develop perpendicular to the direction of minimal effective stress (S_3). The maximum horizontal stress may then either be S_1 or S_2. In a strike-slip environment (like the Southern Volcanic Zone) S_1 and S_3 are horizontal while S_2 is vertical, thus allowing partial melts and fluids to rise in vertical dikes, parallel to S_H. Local features (e.g., gravitational load from the stratovolcanoes and the mountain range as such) may modify the overall stress pattern – this may in turn lead to local deviations of induction vector directions and to slightly different conclusions on anisotropy directions along the 3 profiles in the study area.

Our findings concerning structural anisotropy (if we regard it as a measure of a deeply fractured crust, but being unable to resolve individual dikes/faults due to wavelength considerations) strongly support the assumption of Nakamura (1977) and López-Escobar et al. (1995). The surprising result is, however, that the crust has to be deeply fractured in the forearc as well. Due to low temperatures in the forearc crust the conductive phase cannot be any partial melt here – instead we have to assume a relatively cold, but fluid-rich crust or even, at least partly, an occurrence of metallic phases. The extension of anisotropy beneath the Coastal Cordillera would be in accordance with the broadening of the mid-Tertiary volcanic arc until the Pacific coast, where volcanic outcrops occur south of our actual study area at 41°S (Muñoz et al., 2000). Our results suggest that this magmatic event may have reached even further to the west, beyond the coastline and perhaps until the continental slope.

Unfortunately the model in Fig. 8 explains the impedances only in a crude manner. For the time being we have been unable to construct a model which satisfactorily fits both magnetotelluric and vertical magnetic field observations; this constitutes the next task for the evaluation of the data set. However, several features of the model presented here correspond to the isotropic impedance model (Brasse and Soyer, 2001), in particular the enhanced conductivity below the Central Depression and the generally higher conductivities beneath the volcanic arc. The characteristics of induction vectors outside the area depicted in Figs. 1 and 2 are not known and it would thus be a rewarding effort to establish further sites to the north of the Bío-Bío Fault and to the south in archipelagic Chile.

9 Acknowledgements

We are grateful to the Universidad de Concepción, in particular to K. Bataille, for help in logistical issues. We also acknowledge the contribution to the field measurements by A. Cyganiak, A. Gerner, M. Heigel, A. Manzanares, D. Martens, M. Muñoz, F. Sepúlveda, and T. Worzewski, as well as the support of J. Muñoz (Chilean National Service of Geology and Mining, SERNAGEOMIN) and the National Forest Corporation of Chile (CONAF). We thank J. Pek, J. Cembrano and L.E. Lara for discussions, and P.E. Wannamaker and an anonymous reviewer for constructive comments on the manuscript. Several instruments were supplied by the Geophysical Instrument Pool Potsdam (GIPP); the offshore measurements (which are not taken into account in this paper) were conducted with the help of Woods Hole Oceanographic Institution (A. Chave). Most plots were prepared with the GMT package of Wessel and

Smith (1998). This is manuscript GEOTECH-327 of the R&D-Programme GEOTECHNOLOGIEN, funded by the German Federal Ministry of Education and Research (BMBF) and the German Science Foundation (DFG).

References

Asch, G., Schurr, B., Bohm, M., Yuan, X., Haberland, C., Heit, B., Kind, R., Woelbern, I., Bataille, K., Comte, D., Pardo, M., Viramonte, J., Rietbrock, A., and Giese, P., 2006. Seismological Studies of the Central and Southern Andes. In: O. Oncken et al. (Editors), The Andes: Active Subduction Orogeny, Frontiers in Earth Sciences, Springer, Berlin, 443-458.

Assumpcão, M., 1992. The regional intraplate stress field in South America, J. Geophys. Res., 97, 11889-11903.

Bohm, M., Lüth, S., Echtler, H., Asch, G., Bataille, K., Bruhn, C., Rietbrock, A., and Wigger, P., 2002. The Southern Andes between 36° and 40°S latitude: seismicity and average seismic velocities, Tectonophysics, 356, 275-289.

Brasse, H., and Soyer, W., 2001. A magnetotelluric study in the Southern Chilean Andes, Geophys. Res. Lett., 28, 3 757-3 760.

Brasse, H., Lezaeta, P., Rath, V., Schwalenberg, K., Soyer, W., and Haak, V., 2002. The Bolivian Altiplano conductivity anomaly, J. Geophys. Res., 107, doi:10.1029/2001JB000391.

Brasse, H., and Eydam, D., 2008. Electrical conductivity beneath the Bolivian Orocline and its relation to subduction processes at the South American continental margin, J. Geophys. Res., 113, doi:10.1029/2007JB005142.

Calder, E.S., Harris, A.J.L., Peña, P., Pilger, E., Flynn, L.P., Fuentealba, G., and Moreno, H., 2004. Combined thermal and seismic analysis of the Villarrica volcano lava lake, Chile, Rev. geol. Chile, 31, 259-272.

Cembrano, J., Hervé, F., and Lavenu, A., 1996. The Liquiñe Ofqui fault zone: a long-lived intra-arc fault system in southern Chile, Tectonophysics, 259, 55-66.

Cembrano, J., Lavenu, A., Yañez, G., Riquelme, R., García, M., González, G., and Hérail, G., 2007. Neotectonics. In: T. Moreno and W. Gibbons (Editors), The Geology of Chile, Geol. Soc., London, 231-261.

Chave, A.D., Constable, S.C., and Edwards, R.N., 1991. Electrical Exploration Methods for the Seafloor. In: M.N. Nabighian (Editor), Electromagnetic Methods in Applied Geophysics, Vol. 2, Soc. Expl. Geophys., Tulsa, 931-966.

Cifuentes, I., 1989. The 1960 Chilean earthquakes, J. Geophys. Res., 94, 665-680.

Egbert, G.D., 1997. Robust multiple-station magnetotelluric data processing, Geophys. J. Int., 130, 475-496.

Eydam, D., 2008. Magnetotellurisches Abbild von Fluid- und Schmelzprozessen in Kruste und Mantel der zentralen Anden, diploma thesis, Fachrichtung Geophysik, FU Berlin.

Folguera, A., Zapata, T., and Ramos, V.A., 2006, Late Cenozoic extension and the evolution of the Neuquén Andes. In: S.M. Kay and V.A. Ramos (Editors), Evolution of an Andean margin: A tectonic and magmatic view from the Andes to the Neuquén Basin (35°– 39°S lat), Geol. Soc. Am. Spec. Paper, 407, doi:10.1130/ 2006.2407(12).

Glodny, J., Echtler, H., Figueroa, O., Franz, G., Grfe, K., Kemnitz, H., Kramer, W., Krawczyk, C., Lohrmann, J., Lucassen, F., Melnick, D., Rosenau, M., and Seifert, W., 2006. Long-Term Geological Evolution and Mass-Flow Balance of the South-Central Andes. In: O. Oncken et al. (Editors), The Andes: Active Subduction Orogeny, Frontiers in Earth Sciences,

Springer, Berlin, 401-428.

Gonzáles-Ferrán, O., 1994. Volcanes de Chile, Instituto Geográfico Militar, Santiago de Chile, 640pp.

Groß, K., Micksch, U., and TIPTEQ Research Group, Seismics Team, 2007. The reflection seismic survey of project TIPTEQ – the inventory of the Chilean subduction zone at 38.2°S, Geophys. J. Int., doi:10.1111/j.1365-246X.2007.03680.x.

Haberland, C., Rietbrock, A., Lange, D., Bataille, K., and Hofmann, S., 2006. Interaction between forearc and oceanic plate at the south-central Chilean margin as seen in local seismic data, Geophys. Res. Lett., 33, doi:10.1029/2006GL028189.

Heise, W., and Pous, J., 2001. Effects of anisotropy on the two-dimensional inversion procedure, Geophys. J. Int., 147, 610-621.

Kapinos, G., and Brasse, H., 2006. An Amphibious Magnetotelluric Experiment at the South Chilean Continental Margin. In: O. Ritter and H. Brasse (Editors), Prot. 21. Koll. Elektromagnetische Tiefenforschung, Haus Wohldenberg, Holle, ISSN 0946-7467, 307-314.

Kapinos, G., 2008. Amphibious magnetotellurics at the South-Central Chilean continental margin, PhD thesis, FU Berlin.

Klotz, J., Abolghasem, A., Khazaradze, G., Heinze, B., Vietor, T., Hackney, R., Bataille, K., Maturana, R., Viramonte, J., and Perdomo, R., 2006. Long-Term Signals in the Present-Day Deformation Field of the Central and Southern Andes and Constraints on the Viscosity of the Earths Upper Mantle. In: O. Oncken et al. (Editors), The Andes: Active Subduction Orogeny, Frontiers in Earth Sciences, Springer, Berlin, 65-89.

Krawczyk, C.M., Mechie, J., Tašárová, Z., Lüth, S., Stiller, M., Brasse, H., Echtler, H., Bataille, K., Wigger, P., and Araneda, M., 2006. Geophysical

623 Signatures and Active Tectonics at the South-Central Chilean Margin. In:
624 O. Oncken et al. (Editors), The Andes: Active Subduction Orogeny, Fron-
625 tiers in Earth Sciences, Springer, Berlin, 171-192.

626 Lara, L.E., Naranjo, J.A., and Moreno, H., 2004. Rhyodacitic fissure eruption
627 in Southern Andes (Cordon Caulle; 40.5°S) after the 1960 (Mw:9.5) Chilean
628 earthquake: a structural interpretation, J. Volc. Geotherm. Res., 138, 127-
629 138.

630 Li, Y., 2002. A finite element algorithm for electromagnetic induction in two-
631 dimensional anisotropic conductivity structures, Geophys. J. Int., 148, 389-
632 401.

633 López-Escobar, L., Cembrano, J., and Moreno, H., 1995. Geochemistry and
634 tectonics of the Chilean Southern Andes basaltic Quaternary volcanism (37-
635 46°S), Rev. geol. Chile, 22, 219-234.

636 Lüth, S., and Wigger, P., 2003. A crustal model along 39°S from a seismic
637 refraction profile – ISSA 2000, Rev. geol. Chile, 30, 83-101.

638 Mackie, R.L., Smith, J.T., and Madden, T.R., 1994. Three-dimensional mod-
639 eling using finite difference equations: The magnetotelluric example, Radio
640 Science, 29, 923-935.

641 Melnick, D., Rosenau, M., Folguera, A., and Echtler, H., 2006. Neogene tec-
642 tonic evolution of the Neuquén Andes western flank (37-39°S). In: S.M. Kay
643 and V.A. Ramos (Editors), Evolution of an Andean margin: A tectonic and
644 magmatic view from the Andes to the Neuquén Basin (35-39°S), Geol. Soc.
645 Am. Spec. Paper, 407, doi:10.1130/2006.2407(04).

646 Muñoz, J., Troncoso, R., Duhart, P., Crignola, P., Farmer, L., and Stern,
647 C.R., 2000. The relation of the mid-Tertiary coastal magmatic belt in south-
648 central Chile to the late Oligocene increase in plate convergence rate, Rev.
649 geol. Chile, 27, 177-203.

Nakamura, K., 1977. Volcanoes as possible indicators of tectonic stress orientation (principle and proposal), J. Volcan. Geotherm. Res., 2, 1-16.

Parada, M.A., López-Escobar, L., Oliveros, V., Fuentes, F., Morata, D., Calderón, M., Aguirre, L., Féraud, G., Espinoza, F., Moreno, H., Figueroa, O., Muñoz, J., Troncoso Vásquez, R., and Stern, C.R., 2007. Andean magmatism. In: T. Moreno and W. Gibbons (Editors), The Geology of Chile, Geol. Soc., London, 115-146.

Pek, J. and Verner, T., 1997. Finite difference modelling of magnetotelluric fields in 2-D anisotropic media, Geophys. J. Int., 128, 505-521.

Ramos, V.A., and Kay, S.M., 2006. Overview of the tectonic evolution of the southern Central Andes of Mendoza and Neuquén (35°−39°S latitude). In: S.M. Kay and V.A. Ramos (Editors), Evolution of an Andean margin: A tectonic and magmatic view from the Andes to the Neuquén Basin (35°−39°S), Geol. Soc. Am. Spec. Paper, 407, doi:10.1130/2006.2407(01).

Reuther, C.D, and Moser, E., 2007. Orientation and nature of active crustal stresses determined by electromagnetic measurements in the Patagonian segment of the South America Plate, Int. J. Earth Sci. (Geol. Rundschau), doi: 10.1007/s00531-007-0273-0.

Rietbrock, A., Haberland, C., Bataille, K., Dahm, T., and Oncken, O., 2005. Studying the seismogenic coupling zone with a passive seismic array, EOS Trans. AGU, 86, 293.

Rodi, W., and Mackie, R.L., 2001. Nonlinear conjugate gradients algorithm for 2-D magnetotelluric inversions, Geophysics, 66, 174-187.

Rosenau, M., Melnick, D., and Echtler, H., 2006. Kinematic constraints on intra-arc shear and strain partitioning in the southern Andes between 38°S and 42°S latitude, Tectonics, 25, doi:10.1029/2005TC001943.

Scherwath, M., Flueh, E., Grevemeyer, I., Tilmann, F., Contreras-Reyes, E.,

677 and Weinrebe, W., 2006. Investigating Subduction Zone Processes in Chile,
678 EOS Trans. AGU, 87, 265.

679 Shaw, H., 1980. Fracture mechanisms of magma transport from the mantle
680 to the surface. In: R B. Hargraves (Editor), Physics of magmatic processes,
681 Princeton Univ. Press.

682 Sick, C., Yoon, M.-K., Rauch, K., Buske, S., Lüth, S., Araneda, M., Bataille,
683 K., Chong, G., Giese, P., Krawczyk, C., Mechie, J., Meyer, H., Oncken,
684 O., Reichert, C., Schmitz, M., Shapiro, S., Stiller, M., and Wigger, P.,
685 2006. Seismic Images of Accretive and Erosive Subduction Zones from the
686 Chilean Margin. In: O. Oncken et al. (Editors), The Andes: Active Subduc-
687 tion Orogeny, Frontiers in Earth Sciences, Springer, Berlin, 147-169.

688 Siemon, B., 1997. An interpretation technique for superimposed induction
689 anomalies, Geophys. J. Int., 130, 73-88.

690 Smith, J.T., 1997. Estimating galvanic-distortion magnetic fields in magne-
691 totellurics, Geophys. J. Int., 130, 65-72.

692 Soyer, W., and Brasse, H., 2001. A magneto-variation array study in the cen-
693 tral Andes of N Chile and SW Bolivia, Geophys. Res. Lett., 28, 3023-3026.

694 Soyer, W., 2002. Analysis of geomagnetic variations in the Central and South-
695 ern Andes, PhD thesis, FU Berlin.

696 Soyer, W., and Unsworth, M., 2006. Deep electrical structure of the northern
697 Cascadia (British Columbia, Canada) subduction zone: Implications for the
698 distribution of fluids, Geology, doi:10.1130/G21951.1.

699 Stern, C.R., 2004. Active Andean volcanism: its geologic and tectonic setting,
700 Rev. geol. Chile, 31, 161-206.

701 Sylvester, A.G., 1988. Strike-slip faults, Geol. Soc. Am. Bull., 100, 1666-1703.

702 Völker, D., Wiedicke, M., Ladage, S., Gaedicke, C., Reichert, C., Rauch, K.,
703 Kramer, W., and Heubeck, C., 2006. Latitudinal Variation in Sedimentary

Processes in the Peru-Chile Trench off Central Chile. In: O. Oncken et al. (Editors), The Andes: Active Subduction Orogeny, Frontiers in Earth Sciences, Springer, Berlin, 193-216.

Weidelt, P., 1999. 3-D Conductivity Models: Implications of Electrical Anisotropy. In: M. Oristaglio and B. Spies (Editors), Three-Dimensional Electromagnetics, Soc. of Expl. Geophys., Tulsa, 119-137.

Wessel, P., and Smith, W.H.F., 1998. New, improved version of the Generic Mapping Tools released, EOS Trans. AGU, 79, 579.

Wiese, H., 1962. Geomagnetische Tiefentellurik Teil II: Die Streichrichtung der Untergrundstrukturen des elektrischen Widerstandes, erschlossen aus geomagnetischen Variationen, Pageoph., 52, 83-103.

Yuan X., Asch, G., Bataille, K., Bock, G., Bohm, M., Echtler, H., Kind, R., Oncken, O., and Wölbern, I., 2006. Deep seismic images of the southern Andes. In: S.M. Kay and V.A. Ramos (Editors), Evolution of an Andean margin: a tectonic and magmatic view from the Andes to the Neuquén Basin (35°-39°S lat), Geol. Soc. Am. Spec. Paper, doi:10.1130/2006.2407(03).

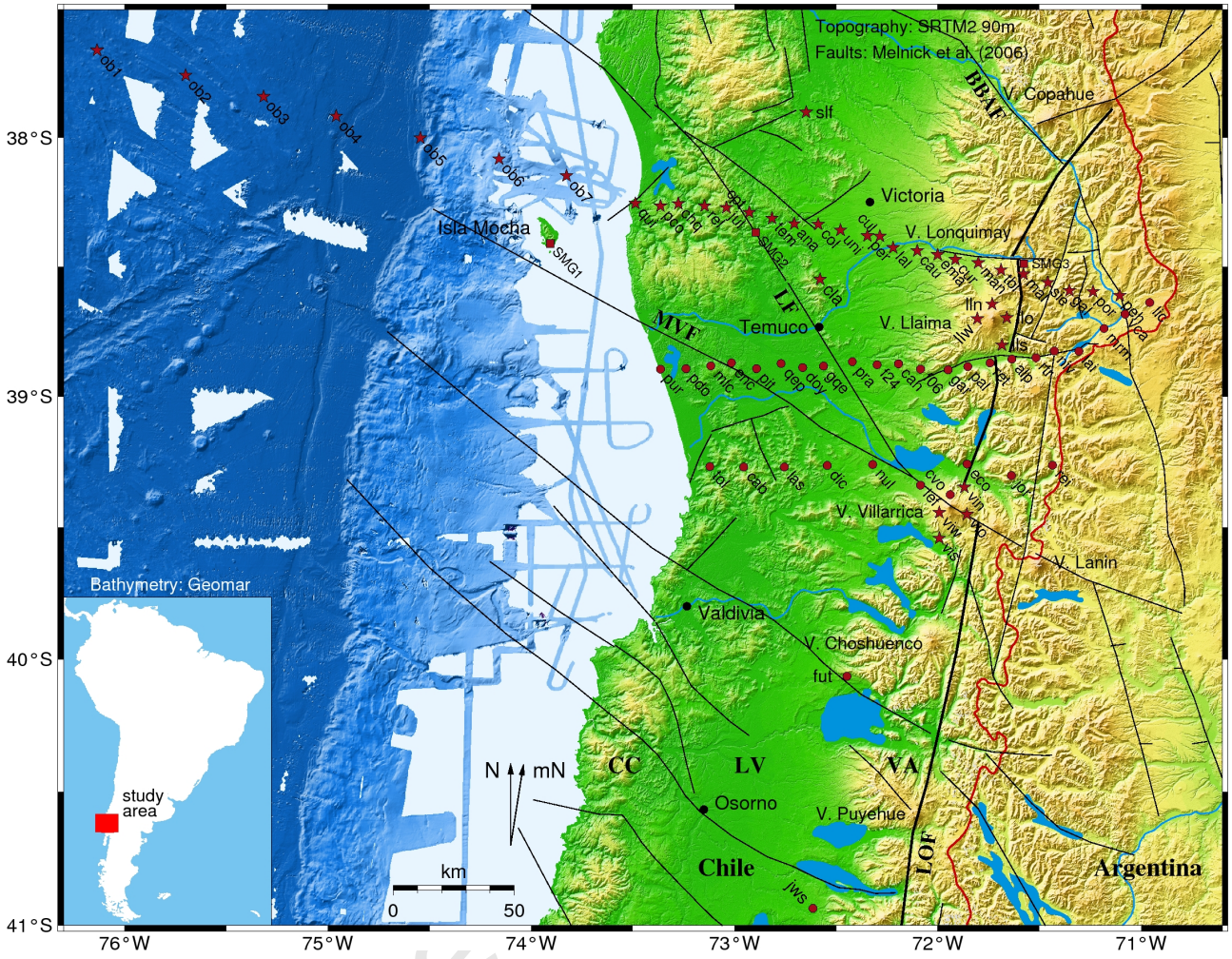

Fig. 1. Shaded relief map of the study area at the South Chilean margin. Topography is based on SRTM (NASA), swath bathymetry is from various cruises of R/V Sonne (Scherwath et al., 2006), fault traces (black lines) are modified from Melnick et al. (2006). Faults mentioned in the text: LOF Liquiñe-Ofqui, LF Lanalhue, MVF Mocha-Villarrica and BBAF Bío-Bío-Aluminé Fault, respectively. CC denotes Coastal Cordillera, LV Longitudinal Valley, VA volcanic arc; mN is magnetic north with a declination of 10°E from geographic N. Stars indicate sites from recent campaign 2004/2005, circles from 2000; SMG1-3 are monitoring sites operated by GFZ Potsdam.

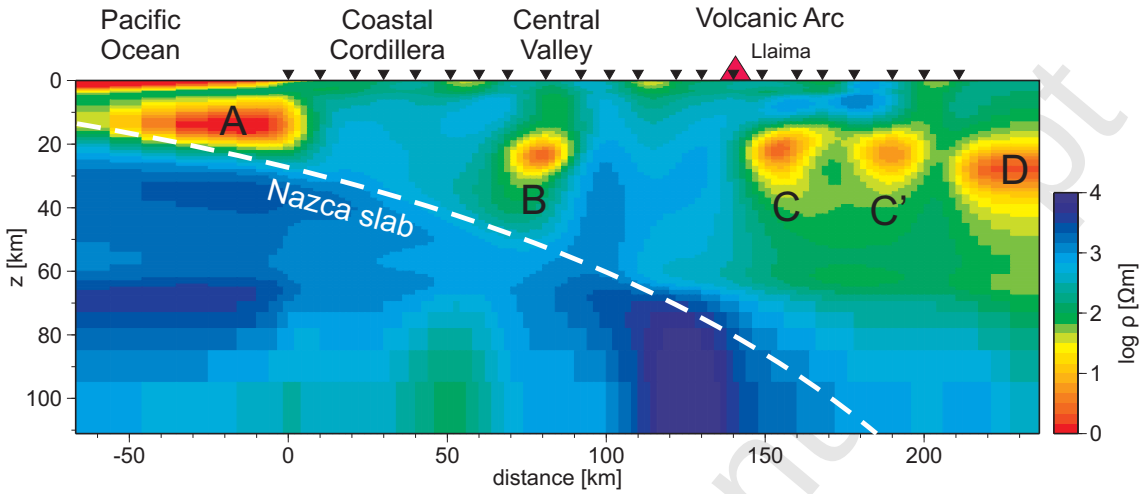

Fig. 2. 2-D model for the central profile, obtained by jointly inverting for TE and TM mode app. resistivities and phases as well as tipper. The model is similar to that of Brasse and Soyer (2001) with the exception of the westernmost conductor A west of the profile, which appears if exact bathymetry (Scherwath et al., 2006) is taken into account. B is the conductor associated with the Lanalhue Fault, C is beneath the volcanic front (just south of Llaima volcano, which erupted again in 2008), C' is a minor conductor at the eastern margin of the Principal Cordillera (volcanic arc) and D is a conductor already in the backarc of Argentina, probably associated with volcanism in the Loncopué Trough. The subducted slab – entered as a homogeneous poor conductor (resistivity 1000 Ωm) in the start model – is broken into more and less resistive domains. For resolution and further explanation see text.

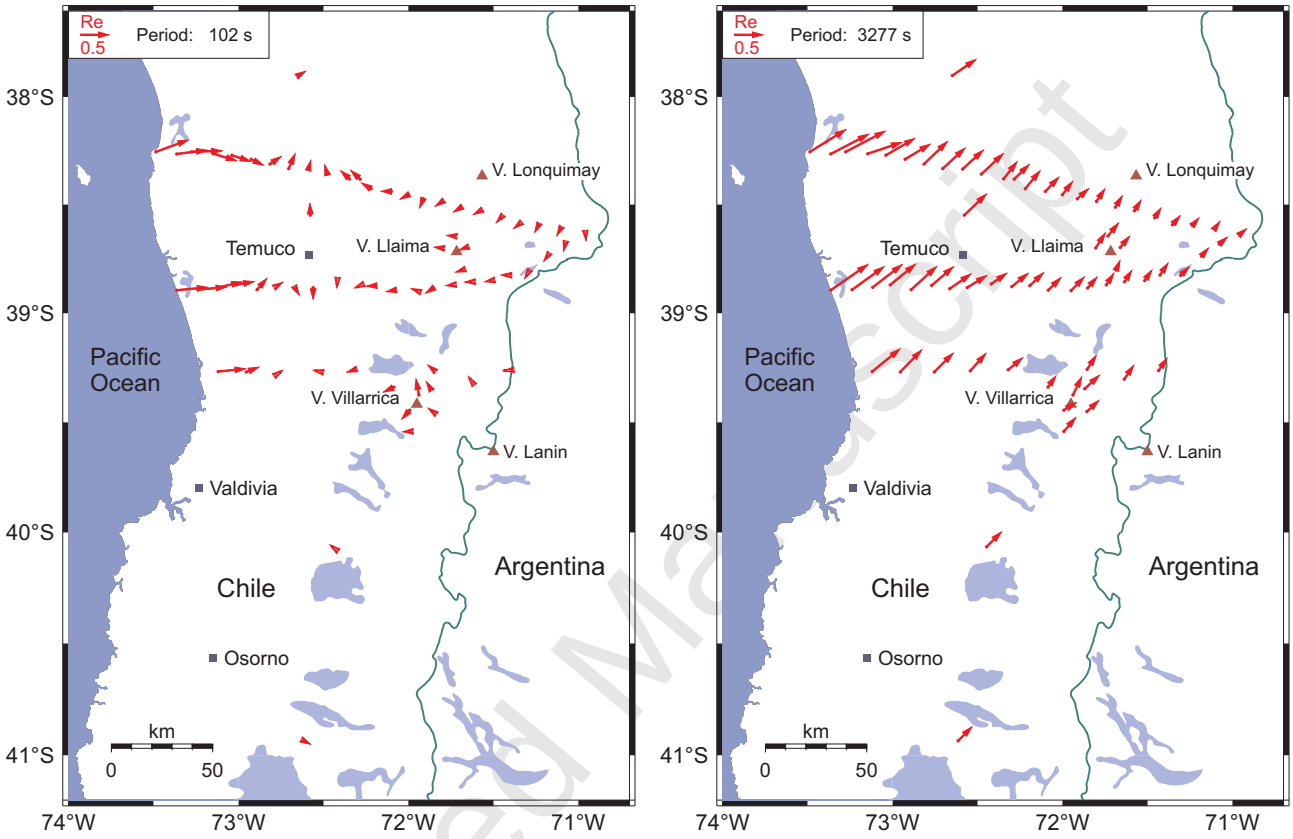

Fig. 3. Real induction vectors in South Chile from two campaigns in 2000 and 2004/2005. Left: At 102 s they display the coast effect near the Pacific Ocean and several local anomalies, particularly around Villarrica volcano in contrast to Llaima volcano, which does not show an effect (the latter data were obtained in early 2005). Right: Deflection of vectors at a period of 3 277 s from the expected W-E direction over the entire study area.

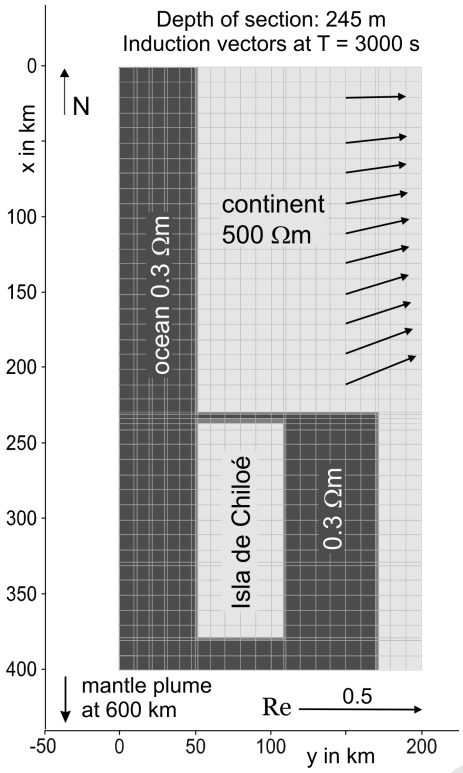

Fig. 4. Plan view of 3-D test model (no. 3 in text) at a depth of 245 m. Real induction vectors at a period of 3 000 s are simulated for a N-S profile in the Longitudinal Valley. The model comprises the ocean, the island of Chiloé, the Gulf of Ancud, and a deep mantle anomaly in the area of the triple junction 200 km to the south of the plot margin. This class of 3-D models may not explain induction vectors in the northern study area.

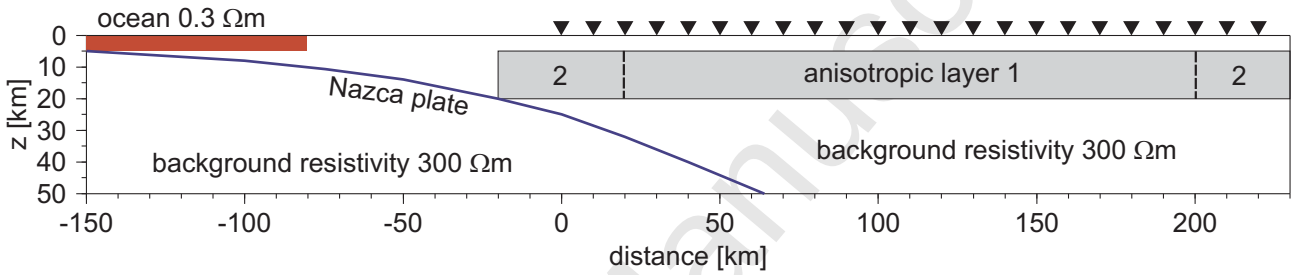

Fig. 5. Principle 2-D models incorporating the Pacific Ocean and an anisotropic layer in the upper crust. (1) The anisotropy is bounded on both sides in EW direction. (2) Layer is extended to the W and unbounded to the E. The top of the downgoing Nazca plate is outlined by a blue line, positions of receivers, where responses are calculated, are indicated by inverted triangles. For parameters see text.

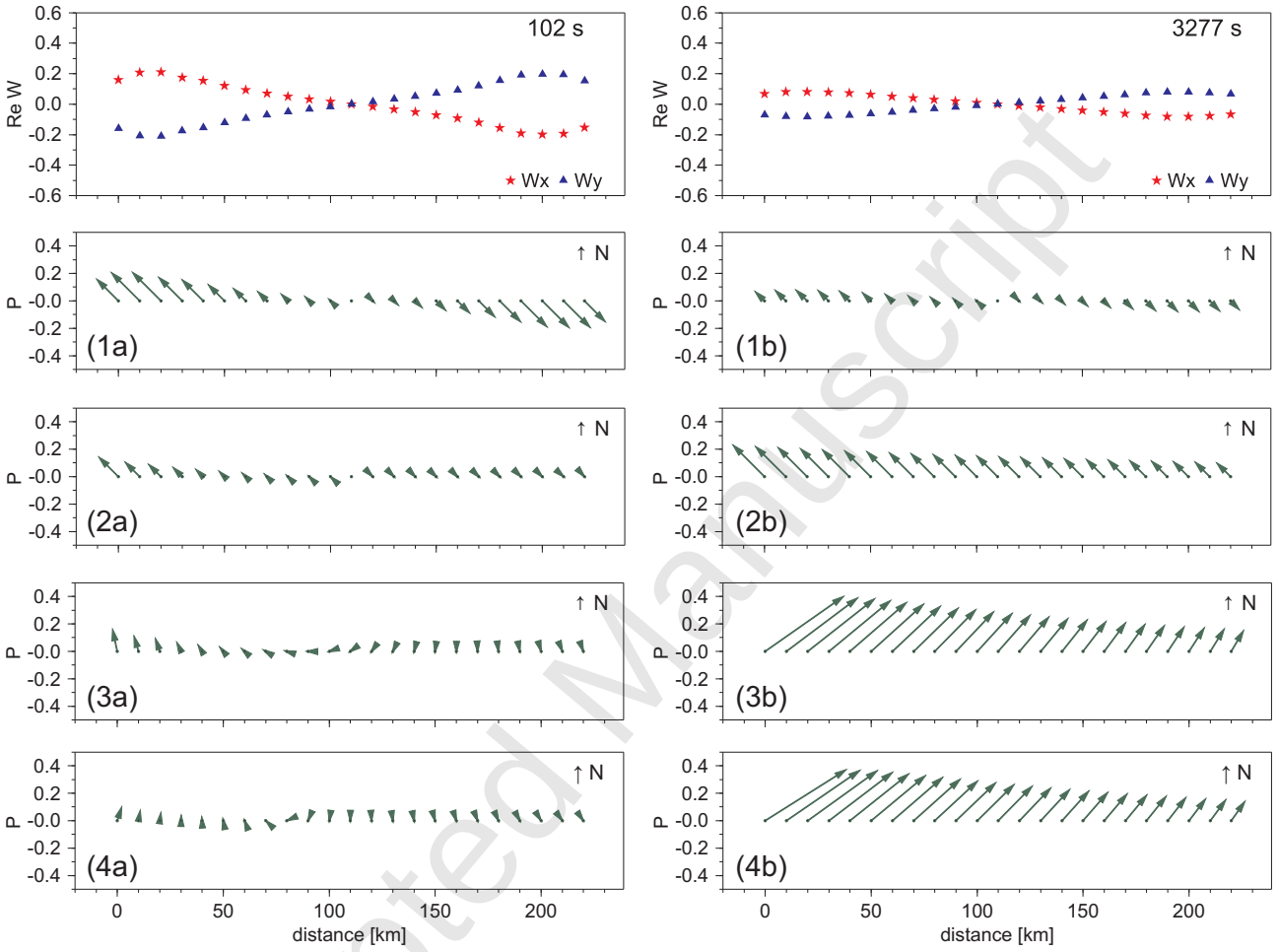

Fig. 6. Response (tipper) of the models from Fig. 5; left for 102 s, right for 3 277 s. Re W is the real part of tipper transfer function, P denotes real-valued induction vector. (1) Bounded anisotropic layer with W_x and W_y on top, (2) layer unbounded to the E, (3) unbounded layer, now with ocean, and (4) as (3), but layer in lower crust. For further explanation see text.

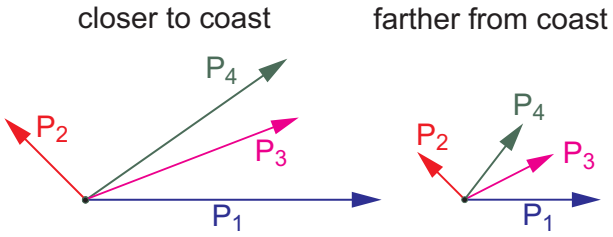

Fig. 7. Induction vectors near (left) and farther (right) from the coast. P1: vector originating from the coast effect above an otherwise homogeneous and isotropic halfspace, P2: from the anisotropic layer, P3: vector addition of P1 and P2, P4: correct vector with modeled anisotropy.

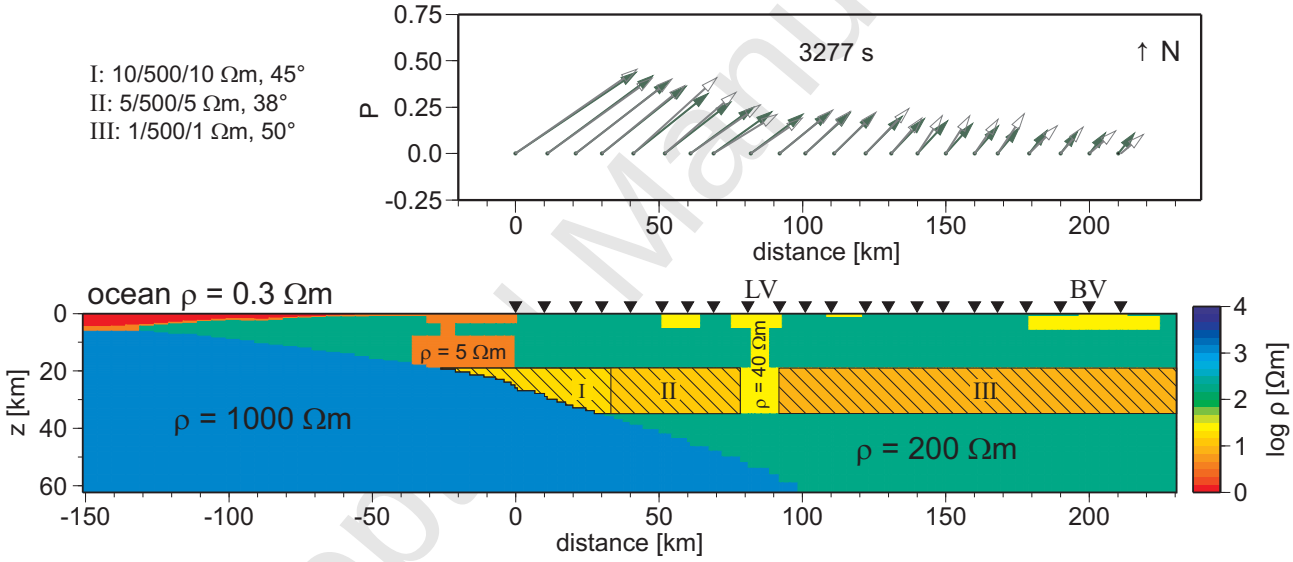

Fig. 8. 2-D anisotropic model yielding the (so far) best fitting response. The anisotropic layer is broken by an isotropic block; in addition the sediments of the Longitudinal Valley (LV) and below the Bío-Bío river (BV) are introduced as a good conductor. Upper left corner shows resistivities of anisotropic blocks in principal directions and strike angle. Upper right: Comparison of model response (filled arrows) with data (open arrows) for the real part of induction vectors at 3277 s along the profile.

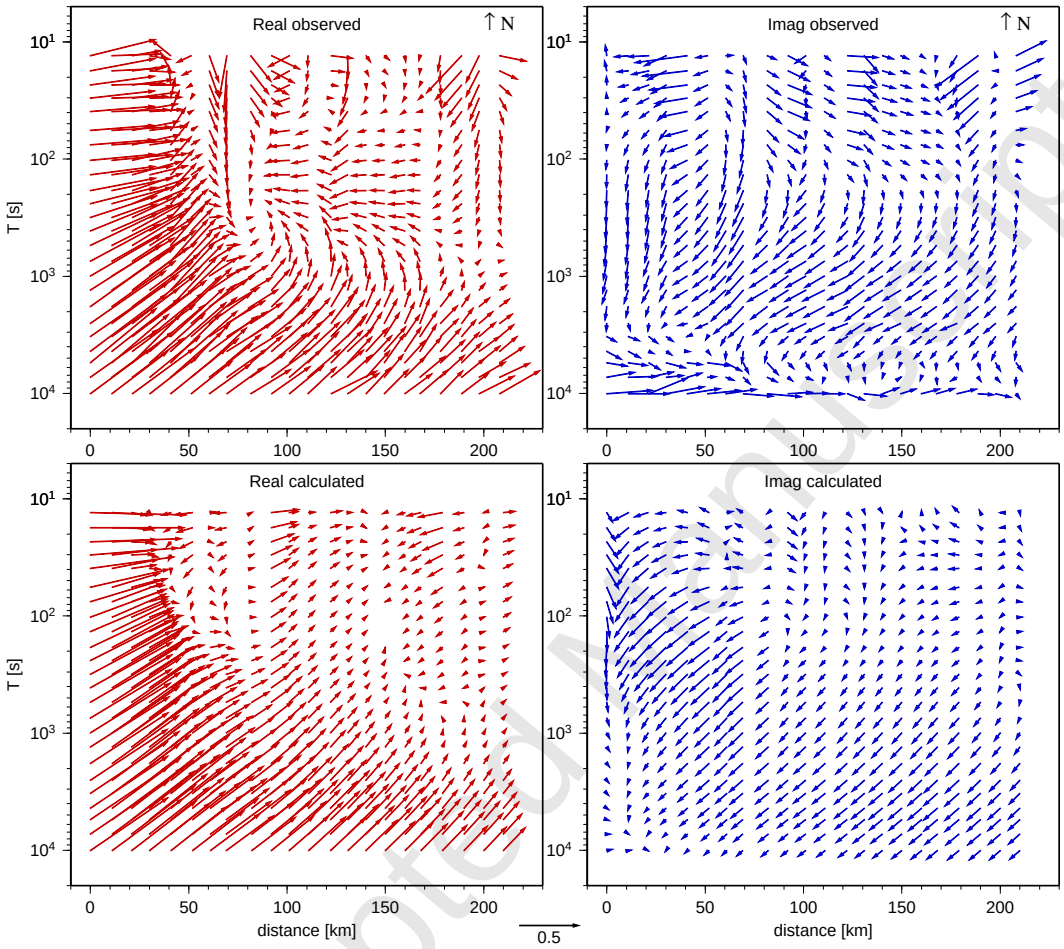

Fig. 9. Comparison of model response (bottom) with data (top) for all periods along the profile (left: real, right: imaginary parts). The model reproduces the main tendency of real and imaginary tipper components with the exception of short-period data, which are distorted by local, probably 3-D effects.